Bicontinuous Microdomain Morphology of Block Copolymers. 1. Tetrapod-Network Structure of Polystyrene–Polyisoprene Diblock Polymers†

Hirokazu Hasegawa, Hideaki Tanaka, Komei Yamasaki,‡ and Takeji Hashimoto*

Department of Polymer Chemistry, Faculty of Engineering, Kyoto University, Kyoto 606, Japan. *Received July 16, 1986*

ABSTRACT: A highly ordered bicontinuous morphology was found for polystyrene–polyisoprene (PS–PI) diblock polymers. The microdomain morphology of PS–PI diblock polymers cast from solution with toluene depends on the copolymer composition but little on the molecular weight. Bicontinuous morphology can be found when the volume fraction of PS component is in a narrow range between 0.62 and 0.66, which is located between the lamellar and cylindrical morphologies. Via electron microscopy of the block polymers with bicontinuous morphology, it has been clarified that the structural unit is a "tetrapod" composed of four short rodlike elements of PI phase. The tetrapod units are linked together to form highly ordered three-dimensional networks and the PS phase fills the matrix. Out of three crystallographic lattices considered for such a network structure ("tetrapod-network structure") the most probable model suggested by the electron microscopic observations is the double-diamond lattice, which coincides with the OBDD structure of the star block polymers reported by Thomas et al. The dependence of the domain spacings and the domain sizes on the molecular weight obeys the two-thirds power law. The block polymers with bicontinuous morphology can form other types of microdomain morphologies such as lamellae, cylinders, and spheres when selective solvents are used for film casting. "Tetrapod-network structure" is considered a general morphology for the microphase separation of block polymers.

1. Introduction

It has been known that there exist three types of fundamental morphologies for the microdomain structure of block polymers such as polystyrene–polyisoprene diblock polymers, i.e., spherical domain structure with cubic lattice, hexagonally packed cylindrical domain structure, and alternating lamellar structure. A total of five different morphologies exist as represented by Molau,[3] including the complementary domain structure for spherical and cylindrical morphologies. The variation in morphology originates from the thermodynamical requirement associated with the incompressibility of polymeric liquids, i.e., the demand of uniform filling of the segments in domain space with the minimum free energy, while keeping the segmental density of each domain equal to the segmental density of the respective bulk homopolymers.[4–7] If the component of the radius of gyration of the A-block chain parallel to the interface is similar to that of the B-block chain for AB diblock polymers, interfaces of zero curvature (or infinite radius) are preferred in order to achieve uniform segmental distribution in domain space with the minimum free energy and the lamellar microdomains result. However, if the component of the radius of gyration parallel to the interface differs for the A-block and B-block chains, uniform packing of block chains in domain space with minimum free energy is possible only when the interfaces have a finite curvature resulting in the formation of cylindrical or spherical microdomains. Thus the morphology changes in order of A spheres, A cylinders, AB lamellae, B cylinders, and B spheres as the fraction, and hence the relative molecular volume of A component in AB block polymer increases. The morphological changes will be observed also by changing the selectivity of the casting solvent for the A component in solution-cast films or in ordered solutions,[8–11] simply because selectivity changes the ratio between the effective radii of gyration of A- and B-block chains. As far as the morphology of the microdomains is concerned, experimental and theoretical studies of microphase separation have been carried out only in this category of five morphologies.

Since the early 1970s it has been known in our laboratory that some polystyrene–polyisoprene diblock polymers exhibit a peculiar and extremely complex morphology that does not belong to any of the five morphologies. Namely, it was clearly seen under an electron microscope that both the polystyrene and the polyisoprene phases were continuous and formed an interpenetrating network structure (or bicontinuous structure). This microdomain structure was highly ordered and reproducible on solvent casting these block polymers. We found such bicontinuous structures not only in the diblock polymers but also in a tricomponent pentablock polymer of I–S–I–A–I type, i.e., polyisoprene-*block*-polystyrene-*block*-polyisoprene-*block*-poly((4-vinylbenzyl)dimethylamine)-*block*-polyisoprene and reported it in 1983 at the 32nd Polymer Symposium of the Society of Polymer Science, Japan,[12] where we considered a single diamond lattice as a possible model for the bicontinuous structure. Those block polymers had a relatively large molecular weights ($M_n \gtrsim 10^5$) and hence had microdomain structures of a size comparable to the thickness of the ultrathin section for the electron microscopic observation, so that it was difficult to observe the three-dimensional symmetry by the specimen tilting technique. Nevertheless, the high molecular weights were a great advantage because the morphological unit of the microdomain was clearly seen under an electron microscope. The structural repeat unit was composed of four short, identical, rodlike elements joined together to form a regular tetrahedron. Because of the characteristic appearance of its morphological unit, we named this microdomain the "tetrapod-network" structure. Then the next problem for us was how to find a three-dimensional structure (or symmetry) that this tetrapod unit can make. There exist only three possibilities in the three-dimensional continuous structures constructed by the tetrapod units: (i) wurtzite, (ii) single diamond, and (iii) double diamond. Detailed examination of the micrographs, which is the essential part of this paper, suggests that the double-diamond structure is the most probable one.

Another example of a new microdomain morphology that does not belong to the five morphologies has also been

† Presented in part before the 34th Annual Meeting, the Society of Polymer Science, Japan, May, 1985.[1]

‡ Present address: Polymer Research Laboratory, Idemitsu Petrochemical Co. Ltd., Anegasaki, Ichihara, Chiba 299-01, Japan.

0024-9297/87/2220-1651$01.50/0

found in star block polymers. The electron micrograph of an ultrathin section that exhibited a "wagon-wheel" image was first reported in 1976 by Aggarwal[13] for a polystyrene–polyisoprene star (or radial) block polymer prepared by Fetters.[14] Recently Alward et al.[15] claimed that the polystyrene–polyisoprene star block polymers exhibiting the wagon-wheel image have a bicontinuous structure by showing the continuity of the polystyrene phase by dynamic mechanical behavior and continuity of the polyisoprene phase by gas sorption behavior. However, the three-dimensional bicontinuity was not shown directly by an electron micrograph. After submission of this paper, a paper on the analysis of the OB structure of the star block polymers by Thomas et al.[2] was published. Their approach to structural analysis was quite different from ours because the "effective molecular weight" (arm molecular weight) of the star block polymers was small ($M_n = 3.3 \times 10^4$) and the morphological unit is much smaller than the thickness of ultrathin sections for the electron microscopic observations. Hence it was difficult to directly find the morphological unit, but it was a great advantage that they could relatively easily find the overall three-dimensional symmetry (cubic symmetry) of the structure. Out of the numerous possible structures that belong to cubic symmetry, they identified the double-diamond lattice by the selective reflections in the small-angle X-ray scattering and the systematic tilt series of the electron micrographs. Thus the bicontinuous microdomain structure of star block polymers was designated as OBDD (ordered bicontinuous double diamond) based on its symmetry. Although the constituent polymer of the diamond networks is different in two cases (polyisoprene for the tetrapod network and polystyrene for the OBDD), we consider that the tetrapod-network structure of the diblock and pentablock polymers and the OBDD structure of the star block polymers are essentially the same type of morphology.

Of the number of block polymers being synthesized and characterized in our laboratory, a remarkable aspect common to these block polymers was found; i.e., the copolymer compositions of the block polymers with the tetrapod-network structure are very close to each other and no other ordinary morphologies were found in this narrow composition range. After examination of the reproducibility of the morphology, we came to the conclusion that the tetrapod-network structure is one of the common morphologies for microphase separation of block polymers and should be recognized in theoretical and experimental studies of block polymers like the other five morphologies.

2. Experimental Section

All polystyrene–polyisoprene (PS–PI) diblock polymers studied in this work were synthesized by living anionic polymerization under high vacuum with sequential addition of styrene and isoprene monomers. The polymerization reactions were carried out at −78 °C using *n*-butyllithium or sec-butyllithium as the initiator and tetrahydrofuran as the solvent. The polyisoprene components of the block polymers, therefore, have a high vinyl content (37–39% 1,2-addition, 57–61% 3,4-addition, and 1–4% 1,4-addition).[16] The film specimens for structural analysis were obtained by casting these block polymer samples at 28–30 °C from 10% solution for the polymers with molecular weights smaller than 2×10^5 and from more dilute solution for the polymers with larger molecular weights. Toluene, which is a mutually good solvent for polystyrene and polyisoprene, was used as the casting solvent for all specimens. The polymer solutions were poured through glass filters into Petri dishes placed on a horizontal bench in a covered, temperature-controlled glass vessel and dried in air until the solvent smell vanished (typically 1 week). The film specimens were further dried in a vacuum oven at room temperature for a week. No further heat treatment was performed.

Table I
Characterization of Polystyrene–Polyisoprene Block Polymers and Microdomain Morphologies of Toluene-Cast Films

sample code	$10^4 M_n$	wt fract PS	vol fract PS, ϕ_{PS}	ref
a. Polyisoprene Spheres in Polystyrene Matrix				
SI-1	7.4	0.84	0.82	18
B-1	8.2	0.83	0.81	
	14.4	0.81	0.79	19
BSI-1	14.5	0.86	0.84	18
B-2	17.6	0.85	0.83	
BSI-8	20.2	0.87	0.85	18
BSI-10	21.9	0.85	0.83	18
SI-21	32.2	0.78	0.76	18
SI-15	65.7	0.78	0.76	18
HS-11	85.0	0.86	0.84	
b. Polyisoprene Cylinders in Polystyrene Matrix				
HS-16	2.2	0.74	0.71	
HS-15	4.2	0.76	0.74	
SI-18	12.1	0.77	0.75	
BSI-9	22.7	0.75	0.73	
HS-6	54.0	0.77	0.75	
BSI-6	56.7	0.78	0.76	
c. Polyisoprene Tetrapod Networks in Polystyrene Matrix				
HY-7	9.56	0.65	0.62	
HY-10	18.6	0.69	0.66	
BSI-3	20.7	0.66	0.63	
d. Polystyrene–Polyisoprene Alternating Lamellae				
SIA-5	2.1	0.53	0.50	20
SIA-4	3.1	0.40	0.37	20
HY-8	3.16	0.48	0.45	
HK-7	3.19	0.35	0.32	
HS-13	3.86	0.35	0.32	
SIA-3	4.9	0.45	0.42	20
HS-10	8.14	0.63	0.60	
SIA-2	10.2	0.61	0.58	20
SI-20	10.5	0.59	0.56	21
HK-3	10.5	0.46	0.43	22
HY-12	52.4	0.52	0.49	23
SI-4	53.8	0.43	0.40	24
HS-9	103.0	0.52	0.49	
e. Polystyrene Cylinders in Polyisoprene Matrix				
HK-6	8.59	0.33	0.30	
HK-4	14.1	0.20	0.18	
HK-5	18.2	0.31	0.28	
f. Polystyrene Spheres in Polyisoprene Matrix				
SI	27.8	0.19	0.17	24

The small-angle X-ray scattering (SAXS) analysis of the microdomain structure of these specimens was performed with a Rigaku Denki X-ray generating unit with a rotating anode and a step-scan goniometer as described in detail elsewhere.[17] A Hitachi H-600S electron microscope was used for the transmission electron microscopy of ultrathin sections of the specimens obtained with an LKB 4800A Ultrotome and stained with osmium tetraoxide.

The microdomain structures were also investigated for the film specimens cast from solution in solvents other than toluene in order to examine the effect of selectivity of the solvent on morphology. The effect of annealing on morphology at various temperatures above glass transition temperature of polystyrene for various lengths of time was tested for some of these specimens.

3. Results and Discussion

3-1. Composition and Molecular Weight Dependence of Microdomain Morphology. The characterizations of the block polymers are listed in Table I. The number-average molecular weight was determined by membrane osmometry. The weight fraction of PS component was assessed from the elemental analysis data.[25] However, the accuracy of the composition characterization decreases as PI content increases. This is because ele-

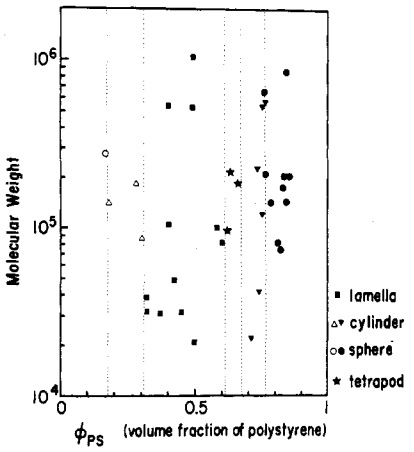

Figure 1. Change of microdomain morphology in toluene-cast films of polystyrene–polyisoprene diblock polymers as a function of total molecular weight and volume fraction of polystyrene component. The morphology is designated by the following symbols: PI spheres, filled circles; PI cylinders, filled triangles; PI tetrapod network, stars; PS–PI lamellae, squares; PS cylinders, open triangles; PS spheres, by open circles.

mental analysis is sensitive to the remaining solvent in samples and requires complete removal of solvent from the block polymer samples. As the PI content increases, the more difficult it becomes.[27] For some of the samples the composition characterization was determined from the ratio of the number-average molecular weight of PS precursor to that of the block polymer when the PS precursor was available. The volume fraction of the PS component was calculated from the weight fraction assuming that the densities of PS and PI microdomains are the same as those of corresponding bulk homopolymers, i.e., 1.052 for PS and 0.925 for PI.[28] The morphologies of the cast films were doubly examined by SAXS analysis and electron microscopy. No discrepancy was found between the results of these two methods.

Figure 1 shows the relation between microdomain morphology of PS–PI diblock polymer films cast from toluene solution and their composition and number-average molecular weight. Morphologies of the microdomains are denoted by symbols. Fewer PI-rich block polymers were prepared than PS-rich block polymers because the ultramicrotomy for electron microscopic observations becomes more difficult with increasing PI content due to the increasing softness of the samples. Consequently only one sample with the morphology of a PS spherical microdomain and a PI matrix was studied.[24] In the examined range of molecular weight (2×10^4–1×10^6), no dependence of morphology on the total molecular weights of the block polymers was observed. The morphology of the microdomain structures solely depends on the composition or the volume fraction of each component as shown by the broken lines in Figure 1. The transition from one morphology to another is markedly sharp. There is no significantly overlapping region of different morphologies along the composition scale. Namely, spherical PI domains in PS matrices were observed with PS volume fraction $\phi_{PS} \gtrsim 0.76$, PI cylinders in PS matrices at $0.76 \gtrsim \phi_{PS} \gtrsim 0.67$, PI tetrapod networks in PS matrices at $0.66 \gtrsim \phi_{PS} \gtrsim 0.62$, PS–PI alternating lamellae at $0.61 \gtrsim \phi_{PS} \gtrsim 0.32$, PS cylinders in PI matrices at $0.30 \gtrsim \phi_{PS} \gtrsim 0.18$, and PS spheres in PI matrices at $0.17 \gtrsim \phi_{PS}$. The limits of PS volume fraction for a particular morphology become less accurate as the PI content increases because of the reason described above. Consequently, the new morphology, the tetrapod-network structure, is located in the very narrow compositional range between the lamellae and the cylinders. The morphology of PS tetrapod-network structures in PI matrices has not yet been found for diblock polymers, but that does not imply that such a morphology does not exist. In fact some examples of such a morphology have been reported for star block polymers.[2,13,15,29] Therefore, there is a possibility that PS tetrapod networks in PI matrices can be found in the compositional range between the lamellae and PS cylinders, i.e., $0.32 \gtrsim \phi_{PS} \gtrsim 0.30$. However, since there is a few percent error in the determination of PS volume fraction in this compositional range, the compositional window might have some uncertainty. Further study is necessary to determine the accurate window for PS tetrapod networks, if it exists. The morphological boundaries in the diagram in Figure 1 are asymmetrical with respect to PS volume fraction. This is considered to be simply due to the asymmetry of the PS–PI block polymers, i.e.; the densities and Kuhn's statistical segment lengths of PS and PI are different.

Sharp transitions between morphologies with varying composition of block polymers and independence of morphology from molecular weight were theoretically predicted by Helfand[30] in the strong segregation limit. In contrast, Leibler[31] predicted that the morphology of block polymers depends on both composition and molecular weight. (In his theory, which can be applied only to the weak segregation limit, the morphology actually depends on the products of degree of polymerization multiplied by the thermodynamical interaction parameter χ between the two components.) Our observations coincide with the former theory.

These theories are, however, based on the assumption of thermodynamic equilibrium. Cast films of PS–PI block polymers, including our case, are not necessarily in their thermodynamical equilibrium. The microdomain structures tend to be frozen-in during the solvent evaporation process.[32] This nonequilibrium effect is most significant in spherical microdomain systems[11,32] and becomes less significant for cylindrical and lamellar microdomains.[9-11] The factors causing the fixation of microdomain structure were discussed in detail previously for spherical microdomains[11] and will be examined elsewhere.[33] After a microdomain structure is formed by complete evaporation of the solvent and if the system is in the strong segregation limit, morphological transitions, e.g., from spheres to cylinders, etc., hardly occur by any practical heat treatment, although the transitions strongly depend on kinetic barriers and hence the molecular weight and χ- parameter.[34] This is true, as will be mentioned later, even in the case of the cast from solution in a selective solvent. Thus, the morphologies of the cast films are those fixed during the course of the solvent evaporation and not necessarily in global thermodynamical equilibrium although local equilibrium (adjustments of domain spacing and domain size for a given domain morphology and for a given interfacial density of the chemical junctions between the two block chains) may be achieved by heat treatment. Therefore, our observations are neither a definite proof of the former theory nor a definite denial of the latter theory. But we have shown the practical trends for designing microdomain structures in terms of composition and molecular weight. To prepare a block polymer having its thermodynamically equilibrium microdomain structure in bulk is experimentally a difficult task.[11,18,32,33]

3-2. Tetrapod-Network Structure. The "tetrapod network" is a bicontinuous structure named after the unique shape of its microdomains. Figure 2 shows an electron micrograph of a ca. 40-nm-thick[35] ultrathin section of an as-cast film of a PS–PI block polymer (sample code:

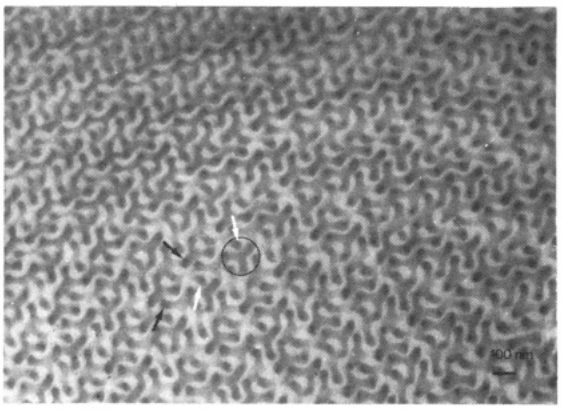

Figure 2. Electron micrograph showing characteristics of tetrapod-like elements in HY-10 film cast from solution in toluene. A tetrapod unit is marked by the circle and the arms perpendicular to the section surface are marked by arrows.

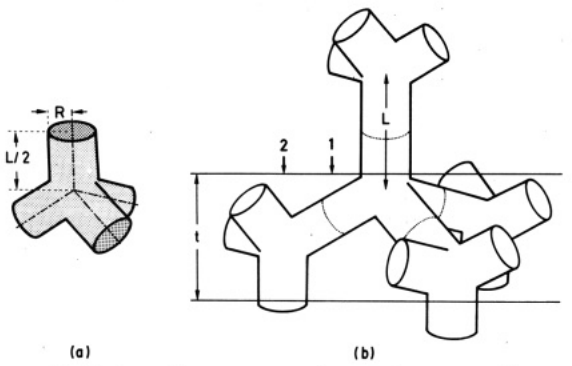

Figure 3. Schematic representation of the tetrapod-network model: (a) a single tetrapod unit; (b) an assembly of five tetrapod units. Two parallel solid lines indicate the surfaces of an ultrathin section with thickness t.

HY-10) that has the tetrapod-network structure. The white area in the micrograph corresponds to the PS phases while the PI phases are stained by osmium tetraoxide and appear dark. The dark PI phases have the shapes of tripods (on the order of 100 nm), consisting of three arms (see the circled area in Figure 2), and these tripods seem to be connected to each other. In other words, the tripod seems to be the structural unit that forms three-dimensional lattice. More careful observation of the micrograph allows us to notice that the structural unit is not a tripod but a tetrapod, as shown in Figure 3a, and that the tetrapod-like structural units are connected to each other to form a three-dimensional network structure as shown in Figure 3b. If the ultrathin section has the thickness designated by t in Figure 3b, the PI microphase observed at position 2 will appear much darker than that observed at position 1 in an electron micrograph because of the difference in the thickness of the PI phase along the electron beam path. In fact, it is clear that there are two stages of darkness in the tripod shape in Figure 2. The darker spots at the outer ends of the tripod arms (as marked by black arrows in Figure 2) indicate the thicker PI phase in the depth direction of the thin section and suggest additional rodlike arms attached upward (or downward) to the tips of the tripods as illustrated in Figure 3b. Since these arms are oriented more or less perpendicular to the section surface, they appear as dark spots in the micrograph. On the other hand, the lighter arms of the tripods seem to lie in the plane more or less parallel to the section surface. Thus the model illustrated in Figure 3 seems to be approximately reasonable. This is the reason the name "tetrapod-network structure" was given to this morphology. The PS phase is the matrix and fills the interstices of the tetrapod-network of PI phase. According to this model both the PS and PI phases, therefore, are continuous in three dimensions; i.e., the tetrapod-network structure is a bicontinuous structure.

Figure 4 is an electron micrograph obtained from a much thicker section (ca. 160 nm thick[35]) of HY-10 film. It is remarkable that the extremely complicated structure shows such high regularity and periodicity with a hexagonal symmetry. A pseudocrystalline structure of microdomains is suggested, as in the cases of the other five morphologies. In addition to it, continuity of the PI tet-

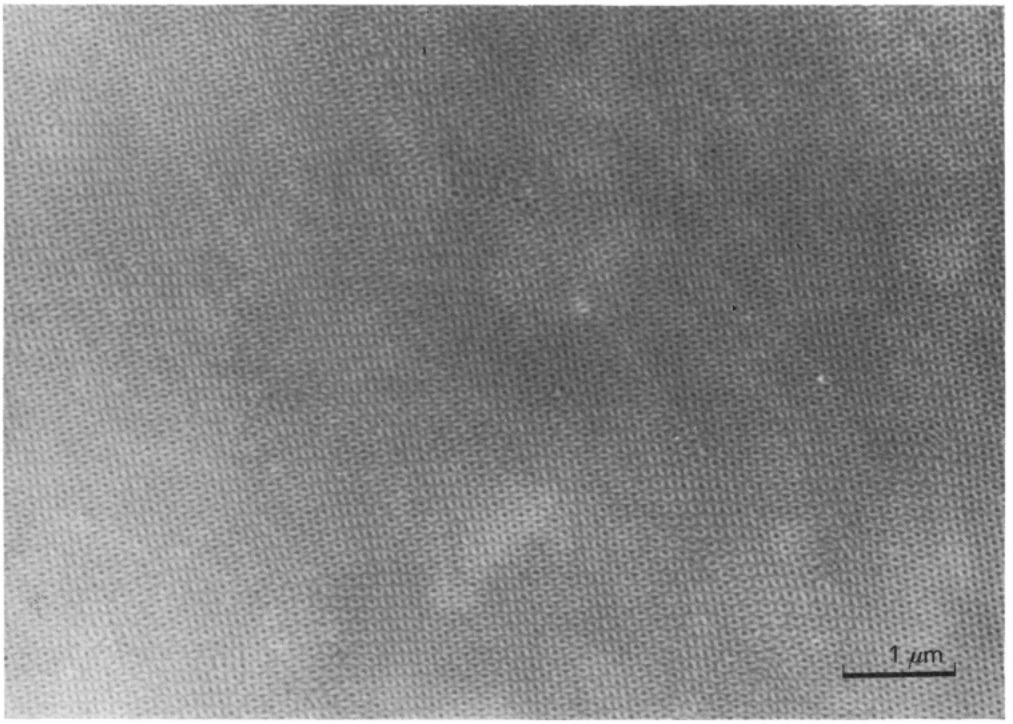

Figure 4. Electron micrograph of the tetrapod-network structure in an HY-10 toluene-cast film showing long-range order with hexagonal symmetry.

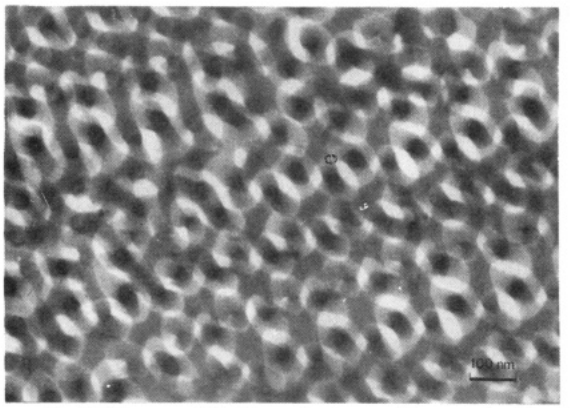

Figure 5. High magnification electron micrograph of a thin section of HY-10 film cast by toluene.

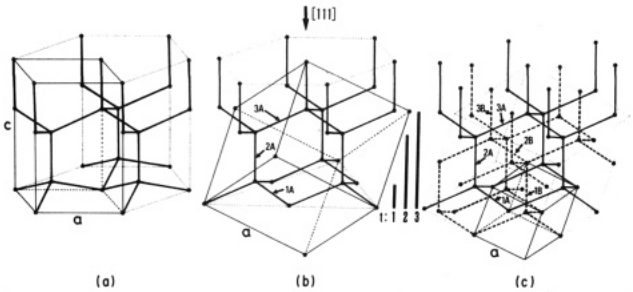

Figure 6. Crystalline lattice models constructed by network structures of tetrapod-like units. Unit cells are indicated by thin solid lines and unit cell dimensions are designated by a and c: (a) wurtzite lattice (hexagonal); (b) single-diamond lattice (cubic); (c) double-diamond lattice (cubic). The numbers 1A–3A and 1B–3B in (b) and (c) correspond to those in Figure 11 and t = 1–3 designates the thicknesses of the thin sections.

rapod network is clearly seen under high magnification (Figure 5) and the bicontinuous structure is visually proved.

3-3. Pseudocrystalline Structure. The pseudocrystalline structure of the tetrapod network was investigated as follows. In the previous section two observations that limit the selection of the lattice structure for the tetrapod-network structure became clear: (1) The structural unit is the tetrapod. (2) The tetrapods are connected together to form a continuous network. There are only three ways to assemble tetrapod units to form periodic network structures in a three-dimensional lattice: *a single-diamond lattice* (SD), *a double-diamond lattice* (DD), and *a wurtzite lattice*. Crystallographically SD and DD belong to cubic systems and the wurtzite lattice belongs to a hexagonal system.

The spatial arrangements of tetrapod structural units are schematically illustrated in Figure 6, parts a and b, for the wurtzite lattice and SD, respectively. The axes of the rodlike arms of the tetrapod units are shown by the thick solid lines. Both models are constructed with the same number of the tetrapod units. The top hexagonal planes in Figure 6, parts a and b, are common to both lattices but the difference in the way of connecting the tetrapod units results in the different shapes of the basal planes. The unit cells are shown by the thin solid lines and the broken lines. A model for the DD is shown in Figure 6c. Its difference from SD is that DD consists of two nonintersecting SD networks, one of which (shown by the thick broken lines in Figure 6c) is translationally shifted in the [110] direction by half the unit cell from the other (shown by the thick solid lines). As a consequence, the unit cell dimension of DD becomes half of the original SD, as shown by the thin solid (for DD) and broken lines (for SD) in Figure 6c, but the cubic symmetry is maintained.

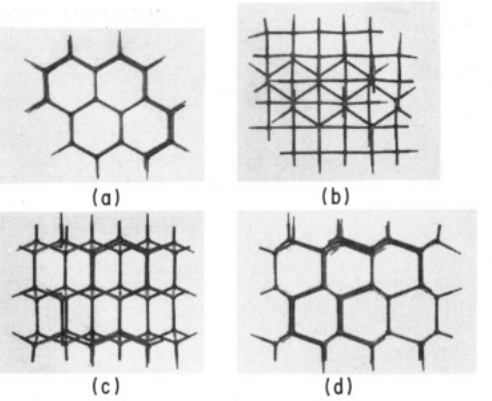

Figure 7. Characteristic views of a wurtzite lattice model from (a) [001], (b) [103], (c) [100], and (d) [110] directions.

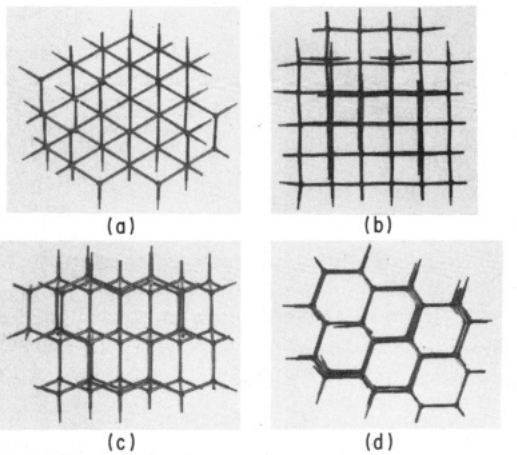

Figure 8. Characteristic views of a single-diamond lattice model from (a) [111], (b) [100], (c) [211], and (d) [110] directions.

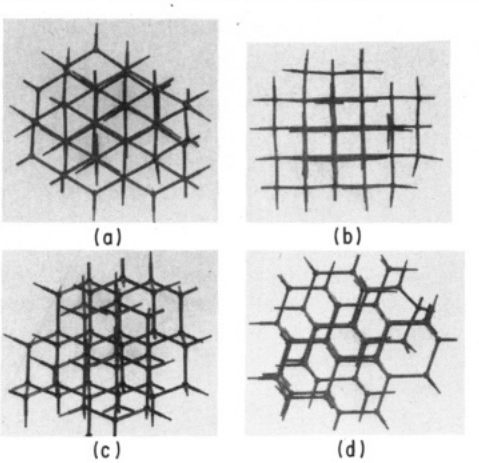

Figure 9. Characteristic views of a double-diamond lattice model from (a) [111], (b) [100], (c) [211], and (d) [110] directions.

Figures 7–9 show the characteristic views of the crystal lattices constructed with a commercial molecular model kit for the wurtzite, SD, and DD structures, respectively. Figure 7 corresponds to the views from the [001], [103], [100], and [110] directions of the wurtzite lattice. Figure 8 is the views from the [111], [100], [211], and [110] directions of the SD lattice. Similarly, Figure 9 shows the views from the [111], [100], [211], and [110] directions of the DD lattice. The figures are arranged in order so that views that resemble each other can be compared between different lattices. Some views are common to two different lattices, but other views are different. This may be a key to determining the correct lattice type of the tetrapod-

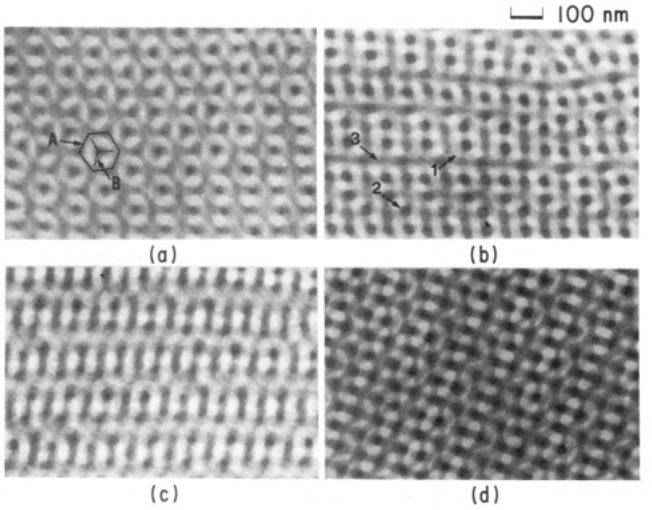

Figure 10. Electron micrographs obtained from thin sections of an HY-10 film cast by toluene showing characteristic images: (a) a "wagon-wheel" image; (b) a square lattice image; (c) a rectangular lattice image with vague and distinct lines; (d) a complicated lattice image with long zigzag lines and short straight lines.

network structure from electron micrographs. For this purpose characteristic views were searched for by looking over wide regions of the ultrathin sections or by tilting[36] the specimens under the electron microscope. It should be noted, however, that the characteristics of these views might change drastically depending on the size of the model (or the thickness of the thin sections in the case of the electron micrographs) relative to the size of the unit cells. For example, if the section thickness t is smaller than the distance L between the centers of two adjacent tetrapod units ($t < L$, t and L being shown in Figure 3), the view from the [111] direction of SD (Figure 8a) will give the same image as Figure 7a. On the other hand, further increase of the section thickness does not change the image from [001] of the wurtzite lattice in Figure 7a. Thus, the model images should be compared with electron micrographs obtained with sufficiently thick sections.

Figure 10 shows electron micrographs of ca. 160-nm-thick sections of HY-10 film with the characteristic appearances. Since the distance L estimated for HY-10 from electron micrographs is smaller than 100 nm, $t > L$. Figure 10a shows a "wagon-wheel" image[37] with hexagonal symmetry which resembles Figure 8a of SD and Figure 9a of DD. Each hexagonal image in Figure 10a (marked A) contains one tetrapod unit (marked B). Three arms of the tetrapod reach every other corner of the hexagon. The other three corners of the hexagon and the center of the tetrapod have dark spots, which suggest that the rodlike arms pointing normal to the section surface are attached to them. The wagon-wheel images of the models in Figures 8a and 9a contain six radial arms, in contrast to three radial arms in the electron micrograph in Figure 10a. This discrepancy can be explained by the effect of the thickness of the thin section as will be discussed in the next paragraph. All of the three models can exhibit a square lattice pattern as shown in Figures 7b, 8b, and 9b, although the wurtzite lattice has additional diagonal units superposed on the square lattice. A clear square lattice image was never found in the electron micrographs. The micrograph shown in Figure 10b resembles the square lattice patterns characteristic of cubic unit cells (as shown in Figures 8b and 9b) and favor the SD or DD model. Diagonal arms (arrow 1 in Figure 10b) found in some squares might suggest the existence of wurtzite linkages in limited regions.

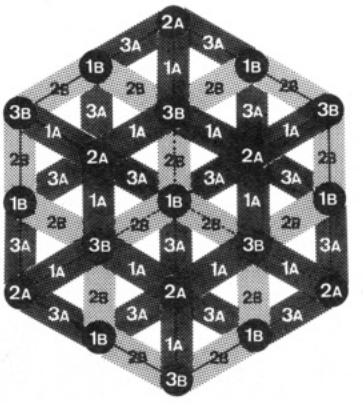

Figure 11. Projection of a double-diamond lattice on the (111) plane. The densely shaded area (designated A) and the lightly shaded area (designated B) indicate the arms of the tetrapods that belong to different sets of networks, A and B, respectively. Solid circles indicate the arms perpendicular to the (111) plane. Numbers indicate the height levels with respect to the (111) plane.

But such a possibility is very small because Figure 10b shows a large distortion. The dark spots (arrow 2 in Figure 10b) at the corners of the squares suggest that the arms of the tetrapods are perpendicular to the section surface, which would not be observed in Figures 7b, 8b, and 9b, in which only line images should be observed. The observation of a line image (arrow 3 in Figure 10b) and dark spots (arrow 2) mixed in the same area suggests local disordering in orientation of the tetrapod units, probably caused by distortion of the lattice structure. This is considered to be the nonequilibrium effect occurring during the deswelling process of film casting and will be discussed later. The micrograph in Figure 10c resembles those of Figures 7c and 8c. The distinct vertical lines in Figure 10c correspond to the vertical arms that lie on the straight lines in Figures 7c, while the vague horizontal lines in Figure 10c are attributed to the zigzag arms that extend horizontally in Figures 7c and 8c. It should be noted that Figure 9c would have shown the same image as Figures 7c and 8c if the section were not so thick. Therefore this pattern is common to all of the three models. Figure 10d resembles Figure 9d of DD, although such a pattern is too complicated to analyze in detail. After all, no micrographs suggesting the existence of a honeycomb pattern as shown in Figure 7a (simple hexagonal lattice) or in Figures 7d and 8d (deformed hexagonal lattices) were obtained. Since the simple hexagonal lattice pattern is the most characteristic image for wurtzite lattice, the wurtzite lattice model can be eliminated from consideration by this fact.

To compare SD and DD, the wagon-wheel image was examined in detail. Figure 11 shows the projection of the DD tetrapod network on the (111) plane (see Figure 9a). The densely and lightly shaded regions (designated A and B, respectively) belong to different sets of networks. In the case of SD, only one set of networks, e.g., the A network, should be considered and the other neglected. The filled circles indicate the arms perpendicular to the (111) plane. The thickness of the networks illustrated in Figure 11 is approximately half of the helix repeat in the [111] direction; i.e., six consecutive arms in the [111] direction form one repeat unit of the helix.

Numbers 1–3 in Figure 11 indicate the level of the arms of the tetrapods in the thickness direction, i.e., the centers of arms 1A and 1B are located at the same depth level and so on. The same numbers are also given to the tetrapod arms in Figure 6 for better understanding of the three-dimensional positions of these arms. If the section thickness is as thin as level 1 (or $t = 1$ as shown in Figure

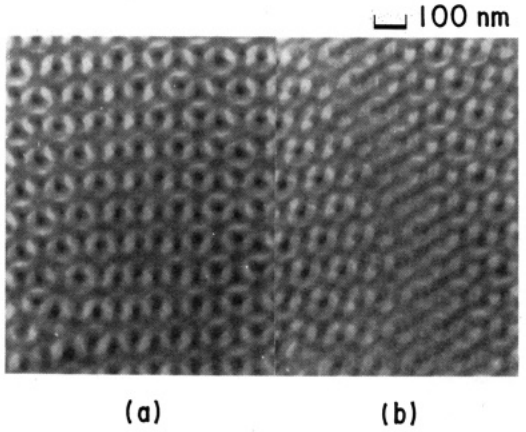

Figure 12. Stereo electron micrographs of thin sections of a HY-10 film cast by toluene. (a) and (b) were tilted by 20° with respect to the vertical axis.

6), a honeycomb pattern that consists of only 1As will be observed for SD under the electron microscope, while a honeycomb pattern with dark spots (1Bs) in the centers will be observed for DD. If the section thickness increases to level 2 (or $t = 2$ as shown in Figure 6), the SD will still show the honeycomb pattern, but the DD should show the wagon-wheel pattern consisting of 1As, 1Bs, 2As, and 2Bs with three 2Bs being radial arms in the hexagon. This wagon-wheel pattern coincides with the electron microscopic image shown in Figure 10a. In order for SD to exhibit a similar wagon-wheel pattern, the section thickness must increase to level 3 (or $t = 3$ as shown in Figure 6). In this case, 1As, 2As, and 3As form a wagon-wheel pattern, with 3As being the radial arms, but it differs in that there is no central dark spot. For the SD, no matter how the section thickness changes the honeycomb pattern with the central dark spots never appears because the three radial arms appear first. On the other hand, the honeycomb pattern with the central dark spots is possible for DD as mentioned above, and Figure 2 shows the indication of such a pattern. In the circle marked in Figure 2, three dark spots (marked by white arrows corresponding to 1Bs in Figure 11) are clearly seen in addition to the tetrapod unit (corresponding to 1As). Thus the DD lattice explains the electron micrographs much better than the other alternatives. It is presumed that the wagon-wheel image with six radial arms as shown in Figure 11 would be observed if much thicker sections than the one used in Figure 10a were used. However, the maximum acceleration voltage, 100 kV, of our electron microscope limits the section thickness used in order to obtain sufficient resolution. The interwoven structure of two sets of tetrapod networks as illustrated in Figure 11 can be more directly recognized by the stereo micrographs shown in Figure 12.[48] Figure 12 is the electron micrographs of the same area from the thin section of HY-10 film (ca. 160 nm thick) tilted by 20°, with the tilt axis being parallel to the vertical direction of the figure. It can be clearly seen that one set of the hexagonal networks is superposed on top of the other. Thus it is concluded that the most probable model for the tetrapod-network structures of PS–PI diblock polymers is a double-diamond lattice. A single-diamond lattice is much less probable and an wurtzite lattice is the least probable.

3-4. An Unsolved Problem. Since the tetrapod network structure is bicontinuous, the morphology of the matrix is of interest. Figure 13 shows an electron micrograph of a thin section of the HY-10 film cast by toluene. The upper left and lower right corners of Figure 13a resemble the view from the [110] direction of the DD model

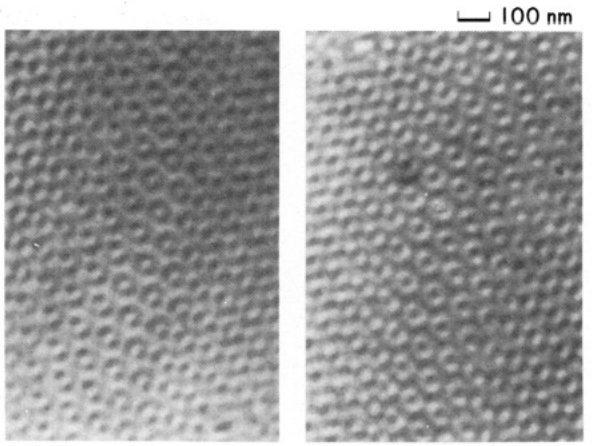

Figure 13. (a) Electron micrograph obtained from a thin section of an HY-10 film cast from toluene. (b) The same area as (a) but the contrast was inverted. The dark area corresponds to the PS phase showing a "wagon-wheel" image.

shown in Figure 9d. The central part of Figure 13a appears different, suggesting a slight change of lattice orientation. Figure 13b shows the same area of the same micrograph, but the contrast was inverted. In other words, the white area corresponds to the PI phase and the dark area corresponds to the PS phase in Figure 13b. The upper left and lower right corners of Figure 13b have exactly the same image as those of Figure 13a, suggesting that the PS phase appears to have a shape similar to the PI phase. Moreover, the central part of Figure 13b shows a wagon-wheel image which is typical of a double-diamond lattice with a PS matrix. In other words the PS matrix is seen as if it also forms double-diamond networks. This is a conflicting idea because the PS phase is supposed to be the continuous matrix which fills the interstices of the PI double-diamond network and cannot be separated into two unconnected networks. This is a puzzling problem and needs further investigation.

3-5. Effect of Molecular Weight. The tetrapod network structure was found in the toluene-cast films of three PS–PI diblock polymers whose characteristics are listed in Table I. Their molecular weights vary from 9.56×10^4 to 20.7×10^4, but their volume fraction of PS component are restricted in a very narrow range, 0.62–0.66. The electron micrographs of their thin sections are shown in Figure 14. The thicknesses of the thin sections were ca. 100 nm for HY-7 (Figure 14a), 160 nm for HY-10 (Figure 14b), and 220 nm for BSI-3 (Figure 14c). Since these thicknesses are greater than the distances between adjacent tetrapods for each sample, wagon-wheel images are observed. It is clearly seen that the domain size (or the size of the wagon wheels) increases as the total molecular weight of the block polymer increases. In Figure 15 the domain spacings, D_{EM} (corresponding to d_{111} of DD lattices), and the radii, R_{EM}, of the rodlike arms of the tetrapods evaluated from the electron micrographs are plotted on a logarithmic scale against respectively the total molecular weight (M_n) and the molecular weight of PI block chains (M_{PI}) that compose the tetrapod networks. For both D_{EM} and R_{EM}, the data points fall on a straight line the slope of which is ca. $^2/_3$, satisfying the two-thirds power law[10,20,32,33,38,39] observed for the other morphologies. Namely

$$D_{EM} \sim M_n^{2/3}$$

$$R_{EM} \sim M_{PI}^{2/3}$$

Figure 14 also suggests that the regularity of the micro-

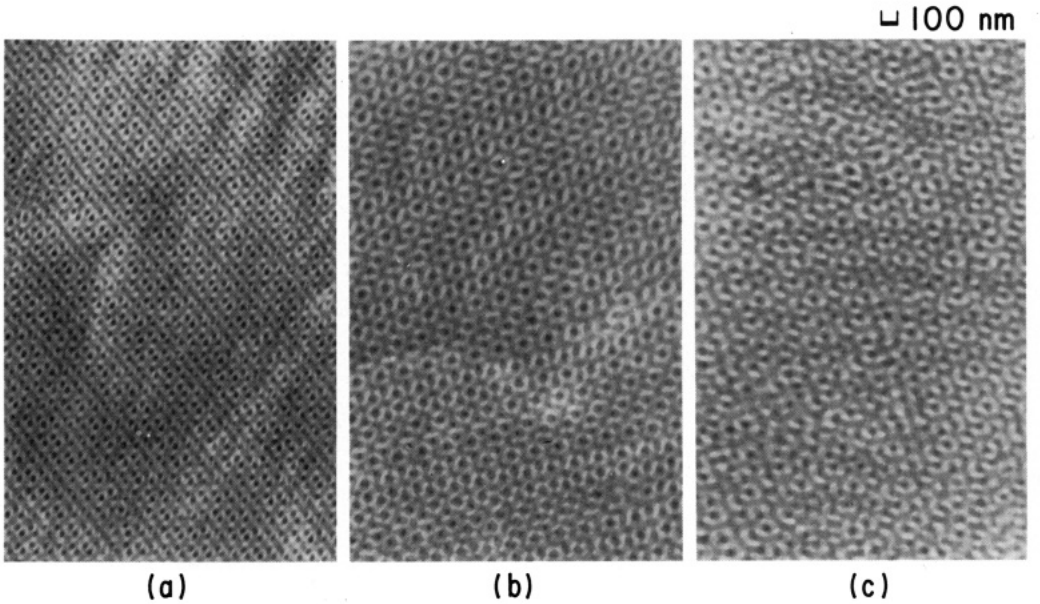

Figure 14. Electron micrographs of thin sections of (a) HY-7, (b) HY-10, and (c) BSI-3 films cast from toluene.

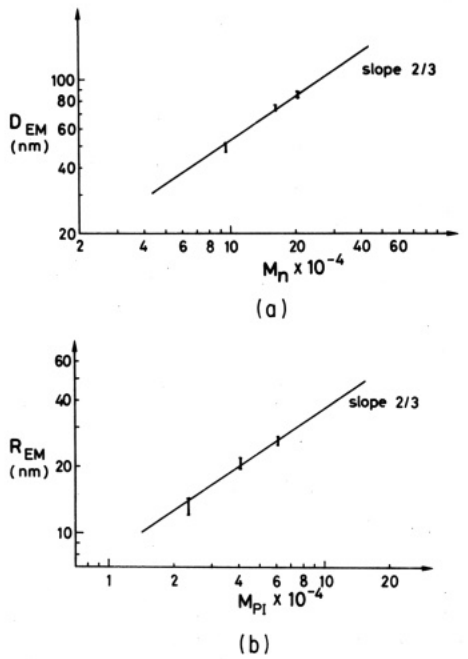

Figure 15. Effect of molecular weight on domain spacing (D_{EM}) and radius of arm (R_{EM}) evaluated from electron micrographs. (a) D_{EM} vs. M_n plot on a logarithmic scale. (b) R_{EM} vs. M_{PI} (molecular weight of PI block chain) on a logarithmic scale.

domain structure decreases with increasing M_n, probably due to the nonequilibrium effect; i.e., the time necessary for the molecular rearrangement during solvent evaporation on film casting increases with increase of the molecular weight and the nonequilibrium state tends to be frozen-in on the completion of film casting.

Another nonequilibrium effect was observed in the cast film of the highest molecular weight sample, BSI-3. Figure 16 shows the cross-section of the polymer–air interface. The observation technique has been reported in detail elsewhere.[40] Near the surface coexistence of two different microdomain morphologies, the tetrapod-network structure (area marked T in the figure) and cylindrical domains (area marked C), was observed. The cylindrical domains were observed only near the surface and never observed in the center of the film. We cannot explain this phenomenon now but we suspect it is the nonequilibrium effect during

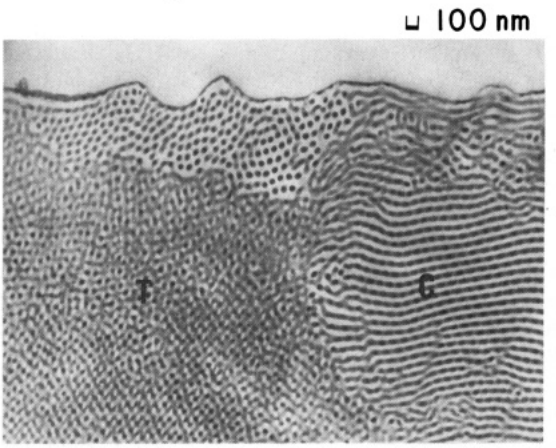

Figure 16. An electron micrograph of a thin section of BSI-3 film cast from toluene showing the air–polymer interface. The area designated by T shows the tetrapod-network mophology while the area designated by C shows the hexagonally-packed cylindrical morphology.

solvent evaporation, which is considered to be the fastest at the surface. The surface of the film is covered with a thin PI phase as previously reported.[40]

3-6. Effect of Casting Solvents on Morphology. In order to examine the effect of the selectivity of the casting solvent on the resulting microdomain morphology in the solvent-cast films, the specimen HY-10, which gives the tetrapod-network morphology by casting with toluene, was cast from cyclohexane, styrene, and 1,4-dioxane solutions. The film casting was carried out slowly under an atmosphere of the corresponding solvent vapor at a constant temperature of 30 °C followed by further removal of the solvent under vacuum at room temperature. Styrene containing a small amount of hydroquinone was used to avoid spontaneous polymerization of styrene.

Figure 17 shows the electron micrographs of these three samples. The microdomain morphology of the cast films apparently depends on the casting solvent. The film cast from cyclohexane solution (Figure 17a) has a lamellar morphology. The film cast from styrene solution (Figure 17b) has a morphology of PI cylinders in a PS matrix. The film cast from 1,4-dioxane solution (Figure 17c) shows a morphology of PI spheres in a PS matrix. In an equilibrium state only one morphology is possible in bulk.

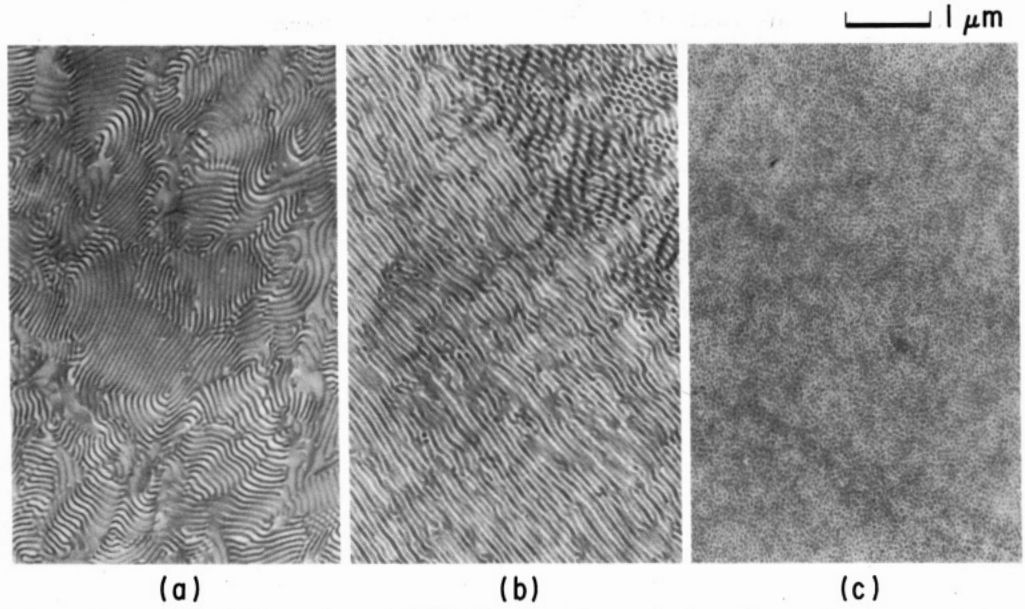

Figure 17. Electron micrographs of thin sections of HY-10 films cast from selective solvents showing a variation of microdomain morphologies: (a) cyclohexane; (b) styrene; (c) 1,4-dioxane.

Therefore, the morphology observed in the cast films is considered to be the memory of the domain structure which existed in solution; i.e., the domain structure in solution is frozen-in sometime during the process of solvent evaporation. The equilibrium domain morphology in solution is expected to vary with the selectivity of the solvent because the solvent affects the relative molecular volume of the constituent block chains. Even annealing of these films at 200 °C for 35 h did not change the original morphologies except for some improvement in regularity of the domain structures examined by electron microscopy.[41] This fact suggests that once-formed microdomains are quite stable and only local equilibrium can be achieved by annealing.

Cyclohexane is a well-known good solvent for polyisoprene but a poor solvent for polystyrene. On the other hand, 1,4-dioxane is a good solvent for polystyrene but a relatively poor solvent for polyisoprene. Toluene and styrene are in-between. The selectivity of the solvents can be compared numerically by the solubility parameters. The reported values of solubility parameters of polymers scatter depending on the investigators and the methods employed. But typical values of solubility parameters for polystyrene and 1,4-*cis*-polyisoprene are 8.5–9.1 and 7.9–8.2, respectively.[42] The solubility parameters of cyclohexane, toluene, styrene, and 1,4-dioxane are 8.2, 8.9, 9.3, and 10.0 $(cal/cm^3)^{1/2}$, respectively.[42] Therefore, the solvent affinity for the polyisoprene component decreases in this order.

The morphology of the microdomain structure of the PS–PI diblock polymer in solution depends upon the dimension of or the component of the radius of gyration of the PS block chain parallel to the interface ($R_{gPS,\parallel}$) to that of the PI block chain ($R_{gPI,\parallel}$). In cyclohexane, $R_{gPS,\parallel}$ and $R_{gPI,\parallel}$ are considered to have about the same magnitude. As the solvent affinity for the PS chains increases (or the solubility parameter becomes larger), $R_{gPS,\parallel}$ increases and $R_{gPI,\parallel}$ decreases, resulting in the situation as schematically illustrated in Figure 18a. Thus, the segmental density becomes high in the PS phase while it becomes low in the PI phase if the system maintains flat interfaces and if the PS and PI chains maintain conformations with maximum conformational entropy. Such a state is energetically unstable. In order to maintain the segmental density of each phase to that of corresponding homopolymer solution, it is necessary either that PS block chains take the conformation extended normal to the interface (Figure 18b) or that the interface has a finite curvature (Figure 18c). The former case results in a significant loss of conformational entropy for the PS block chains while the latter can achieve uniform segmental packing without a significant loss of conformational entropy. The interfacial areas that also contribute to the net free energy may be different for these two cases. Therefore, the energetic balance between the conformational entropy loss and the interfacial energy increase is the factor determining which case is preferred. If the interfacial area is not too different between the two cases, the latter (Figure 18c) will be preferred. Usually a highly extended conformation of PS chains is unlikely and the interface forms a curved surface to result in tetrapod networks, cylinders, and then spheres with increasing solvent selectivity for PS.[43] It should be noted that the chains in the domain space should have an extensive lateral overlap, the aspect of which was ignored in the schematic diagram of Figure 18 in order to simplify the diagram.

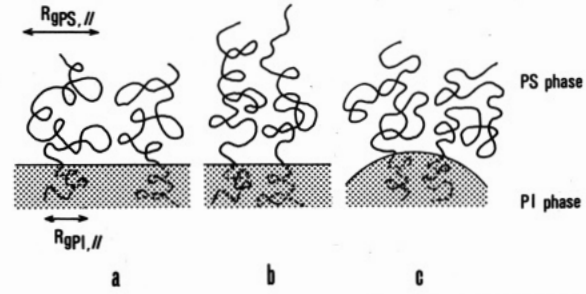

Figure 18. Models of molecular packing of a PS–PI diblock polymer with high PS fraction. (a) A planar interface. A large molecular volume of the PS block chain against a small molecular volume of the PI block chain ($R_{gPS,\parallel} \gg R_{gPI,\parallel}$) results in unbalanced segmental densities in two phases. (b) A planar interface. PS block chains take extended conformation to take the uniform segmental density distribution. ($R_{gPS,\parallel} \simeq R_{gPI,\parallel}$). (c) A curved interface. Uniform segmental density distribution can be achieved with the same conformation as (a).

3-7. SAXS Analysis. The morphology examined by electron microscopy was confirmed by SAXS analysis. Figure 19 shows the SAXS profiles obtained for the same specimens of HY-10 films as those used for electron mi-

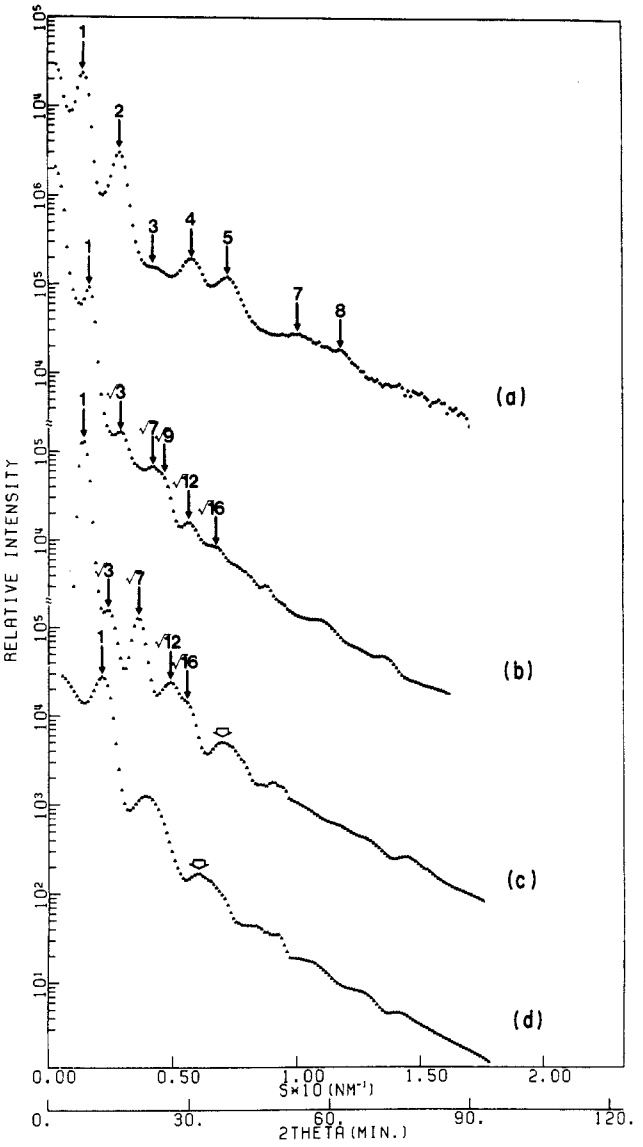

Figure 19. Small-angle X-ray scattering profiles (edge view) from HY-10 films cast from (a) cyclohexane, (b) toluene, (c) styrene, and (d) 1,4-dioxane.

croscopy. Curves a–d correspond to the films cast by cyclohexane, toluene, styrene, and 1,4-dioxane, respectively. The incident X-rays are parallel to the film surfaces, and the scattering intensity distributions normal to the film surfaces (edge profiles) were obtained. The intensity data were desmeared[22] for the slit height and slit width except for the sample cast from cyclohexane solution. The film cast from cyclohexane solution showed an anisotropic SAXS profile with discrete equatorial scattering maxima in the direction normal to the film surface at the scattering angles in the ratios of 1, 2, 4, 5, 7, and 8 as marked in Figure 19, indicating an alternating lamellar structure with a domain spacing of 67.9 nm. The depression of the third and sixth scattering maxima suggests the volume composition of one component being 0.33–0.34,[22] which is in good agreement with the polyisoprene volume fraction of 0.34 obtained from polymer characterization.

SAXS profiles of the films cast from toluene and styrene solutions showed similar behavior; i.e., both of them have scattering maxima at the scattering angles in the ratios of 1, $3^{1/2}$, $7^{1/2}$, etc. Such behavior is usually found in a hexagonally packed cylindrical domain structures. The styrene-cast film has a cylindrical morphology, but the toluene-cast film has a tetrapod-network structure with a double-diamond lattice. The double-diamond structure with the space group $Pn3$ and $Pn3m$ should show scattering maxima at the scattering angles in the ratios of 1, $(^3/_2)^{1/2}$, $2^{1/2}$, $3^{1/2}$, etc.[2] However, the scattering maxima at $(^3/_2)^{1/2}$ and $2^{1/2}$ were not observed. This is probably because the resolution (0.6 min in terms of scattering angle 2θ) of the scattering curve was insufficient for a system with such a large domain spacing as 60.0 nm. Two major peaks, those numbered 1 and $3^{1/2}$ in curve b of Figure 19 are located at 2θ = 8.82 min and 15.6 min, respectively, and there exist only 10 data points in-between. Two unobserved peaks are supposed to be located at 2θ = 10.8 min and 12.5 min, only two data points apart, and their intensities are expected to be weak.[2] In addition to this there is a sharp intensity drop between the first peak and the $3^{1/2}$ peak. Thus it is impossible to resolve the $(^3/_2)^{1/2}$ and $2^{1/2}$ peaks. In order for these peaks to be resolved, the apparatus should have, at least, a spatial resolution better than 2 min and hence 260 nm in spacing. Another possible reason for these two peaks not being observed is that the cubic symmetry of the tetrapod network is lost in the course of film casting by the nonequilibrium effect; i.e., after a certain concentration the film tends to shrink only in the thickness direction due to deswelling because the shrinking in the transverse direction is disturbed by the adhesion of the film onto the glass surface of the Petri dish used for casting and hence the freedom of the block chains to adjust the domain structure to the equilibrium one is lost.[11,18,32,33] Thus, the square lattice observed in the electron micrograph (Figure 10b) is not as regular as expected from the model (Figure 9b), but the hexagonal symmetry remained as observed in the electron micrographs with the wagon-wheel image. The third possibility is the effect of the particle factor. SAXS intensity is given by the product of the lattice scattering intensity multiplied by the particle scattering intensity. The particle scattering from the tetrapod might cause the depression of the two peaks, $(^3/_2)^{1/2}$ and $2^{1/2}$, existing between those numbered 1 and $3^{1/2}$ in Figure 19b. The difference in the relative peak heights of the SAXS profiles from the films cast by toluene and styrene in Figure 19 suggests the difference in their particle factors. One scattering particle is a cylinder and the other is a tetrapod. The lattice spacings of these two structures are slightly different: 60.0 nm for the tetrapod network and 70.0 nm for the cylindrical structure. For the cylindrical microdomains the radius R was calculated from the scattering maximum, indicated by an open arrow in Figure 19, which corresponds to the second maximum (i = 2) of particle scattering of a single cylinder by the equation[18]

$$4\,(R/\lambda)\sin\theta_i = 4.98, 8.364, 11.46, \ldots \quad (\text{for } i = 1, 2, 3, \ldots)$$

where λ is the wavelength of the X-ray and θ_i is the scattering angle of the i-th maximum of the particle scattering. The obtained value R = 18.9 nm agrees fairly well with the value $R = 22 \pm 2$ nm measured from the electron micrograph (Figure 17b).

The 1,4-dioxane-cast film showed a different SAXS profile from the other three. The first scattering maximum corresponds to the domain spacing, and the second scattering maximum is considered to be the higher order (possibly the superposition of $3^{1/2}$ and $4^{1/2}$) peaks. The third intensity maximum, indicated by an open arrow in Figure 19, is probably caused by the particle scattering from a single spherical domain. For the particle scattering from a sphere, the intensity maxima are related to the radius of the sphere by[18]

$4\ (R/\lambda) \sin \theta_i = 5.765, 9.10, 12.3, \ldots$ (for $i = 1, 2, 3, \ldots$)

The obtained value $R = 15.2$ nm ($i = 1$) is in good agreement with the value $R = 17 \pm 2$ nm measured from the electron micrograph (Figure 17c). The spacing of 46.0 nm for the spherical domain structure is considerably small compared with the other three. This is due to the nonequilibrium effect, the morphology being fixed at relatively low concentration.[11] Otherwise, the domain spacings are maintained more or less at a constant value independent of the morphology.

3-8. Generality of the Tetrapod-Network Structure. Bicontinuous microdomain structures were also studied in star block polymers.[2,13,15,29] PS–PI star block polymers with PS segments as the outer component having a weight fraction of 30% were reported to exhibit bicontinuous structures. "Wagon-wheel" images were obtained in the electron micrographs of these star block polymers. Their images are essentially the same as our tetrapod-networks although the contrast is reversed because the composition of their star block polymers is opposite to that of our diblock polymers. The bicontinuous structure of the star block polymers also has a symmetry of double-diamind lattice.[2] Thomas et al. also found a wagon-wheel image in a PS–PB diblock polymer ($M_n = 3.2 \times 10^4$, $\phi_{PS} = 0.65$).[45] The comparison between the diblock polymers and star block polymers with the bicontinuous structure will be reported elsewhere.[46]

The wagon-wheel images observed by electron microscopy were found also in the mixtures of two different PS–PI block polymers,[39] in a tricomponent pentablock polymer of I–S–I–A–I type[12] and in a PI-grafted PS.[47] All of them suggest bicontinuous tetrapod-network structures. Thus it can be concluded that the tetrapod-network structure is a general morphology for the microphase separation of block and graft copolymers.

4. Conclusions

The microdomain morphology of PS–PI diblock polymers in the films cast from solutions in toluene, which is a mutually good solvent for PS and PI components, depends little on the total molecular weight of the block polymers in the range of molecular weight covered in this work ($M_n = 2 \times 10^4$ to 10^6) but very much on the composition of the block polymers. The microdomain morphologies found for block polymers are PI spheres in PS matrices when PS has a volume fraction of $\phi_{PS} \gtrsim 0.76$, PI cylinders in PS matrices when $0.76 \gtrsim \phi_{PS} \gtrsim 0.67$, PI tetrapod-networks in PS matrices when $0.66 \gtrsim \phi_{PS} \gtrsim 0.62$, PS–PI alternating lamellae when $0.61 \gtrsim \phi_{PS} \gtrsim 0.32$, PS cylinders in PI matrices when $0.30 \gtrsim \phi_{PS} \gtrsim 0.18$, and PS spheres in PI matrices when $0.17 \gtrsim \phi_{PS}$.

A new morphology named the "tetrapod-network" structure was found for PS–PI diblock polymers with $0.66 \gtrsim \phi_{PS} \gtrsim 0.62$. It is an entirely different morphology from lamellae, cylinders, and spheres. The tetrapod network is a bicontinuous structure consisting of two interpenetrating diamond networks of interconnected tetrapod-like PI microdomain elements embedded in a PS matrix. A double-diamond lattice model was shown to be the most suitable to explain electron micrographs obtained for ultrathin sections of cast films of these polymers. In contrast to the star block polymers,[2] the SAXS profile from the tetrapod-network structure showed only peaks corresponding to a hexagonal symmetry. This is probably because the spacing of the tetrapod network studied is so large that the fine structure associated with the DD lattice cannot be unequivocally resolved by the present SAXS technique. Alternatively it could be due to the nonequilibrium effect produced during solvent-casting process. The internal strain in the cast film may deform the double-diamond lattice to loose the cubic symmetry.

The morphology of block polymers with the tetrapod-network structure can be changed into lamellar, cylindrical, and spherical microdomain morphologies by changing the casting solvent from toluene (nonselective solvent) to cyclohexane, styrene, and 1,4-dioxane (selective solvents), respectively. The microdomain structures obtained with selective solvents are considered to be nonequilibrium structures in bulk. This phenomenon can be explained by the fixation of the microdomain structure in solution at a certain concentration during the film-casting process. Namely, the microdomain structure in solution which is determined by the relative molecular volumes of PS and PI block chains, and therefore by the casting solvents, is frozen-in in the cast film.[11]

Tetrapod-network structures were also found in block polymer blends,[39] a three-component pentablock polymer,[12] star block polymers,[2,13,15,29] and a graft polymer.[47] Therefore, it is considered to be a general morphology for microphase separation of block and graft copolymers.

Acknowledgment. We thank Professor E. L. Thomas for discussions concerning the OBDD structure in star block polymers. We are grateful to Professor H. Kawai for his encouragement of this work. This work is partially supported by a Grant-in-Aid for Scientific Research from The Ministry of Education, Science and Culture, Japan (00540009).

Registry No. (PI)(PS) (block copolymer), 105729-79-1.

References and Notes

(1) Hasegawa, H.; Hashimoto, T. *Polym. Prep. Jpn.* **1985**, *34*, 775.
(2) Thomas, E. L.; Alward, D. B.; Kinning, D. J.; Martin, D. C.; Handlin, D. L., Jr.; Fetters, L. J. *Macromolecules* **1986**, *19*, 2197.
(3) Molau, G. E. *Block Copolymers*; Aggarwal, S. L., Ed.; Plenum: New York, 1970.
(4) Meier, D. J. *J. Polym. Sci., Part C* **1969**, *26*, 31.
(5) Meier, D. J. *Block and Graft Copolymers*; Burke, J. J., Weiss, V., Eds.; Syracuse University Press: New York, 1973.
(6) Helfand, E.; Wasserman, Z. R. *Macromolecules* **1976**, *9*, 879; **1978**, *11*, 960; **1980**, *13*, 994.
(7) Ohta, T.; Kawasaki, K. *Macromolecules* **1986**, *19*, 2621.
(8) Shibayama, M.; Hashimoto, T.; Kawai, H. *Macromolecules* **1983**, *16*, 16.
(9) Shibayama, M.; Hashimoto, T.; Hasegawa, H.; Kawai, H. *Macromolecules* **1983**, *16*, 1427.
(10) Hashimoto, T.; Shibayama, M.; Kawai, H. *Macromolecules* **1983**, *16*, 1093.
(11) Shibayama, M.; Hashimoto, T.; Kawai, H. *Macromolecules* **1983**, *16*, 1434.
(12) Hasegawa, H.; Sumitomo, T.; Hashimoto, T.; Kawai, H. Presented at the 32nd Polymer Symposium of the Society of Polymer Science, Japan, 1983; *Polym. Prepr. Jpn.* **1983**, *32*, 1695. Hasegawa, H.; Sumitomo, T.; Hashimoto, T., the second paper of this series, to be published.
(13) Aggarwal, S. L. *Polymer* **1976**, *17*, 938.
(14) Fetters, L. J. In *Block Copolymers, Science and Technology*; Meier, D. J., Ed.; MMI Press Symposium Series; MMI Press: Midland, MI 1983, Vol. 3, p 17.
(15) Alward, D. B.; Kinning, D. J.; Thomas, E. L.; Fetters, L. J. *Macromolecules* **1986**, *19*, 215.
(16) Hashimoto, T.; Nakamura, N.; Shibayama, M.; Izumi, A.; Kawai, H. *J. Macromol. Sci., Phys.* **1980**, *B17*, 389.
(17) Todo, A.; Hashimoto, T.; Kawai, H. *J. Appl. Crystallogr.* **1978**, *11*, 558.
(18) Todo, A.; Uno, H.; Miyoshi, K.; Hashimoto, T.; Kawai, H. *Polym. Eng. Sci.* **1977**, *17*, 587.
(19) Inoue, T.; Ishihara, H.; Kawai, H.; Ito, Y.; Kato, K. Presented at the International Conference on Mechanical Behavior of Materials, Kyoto, Aug 17, 1971.
(20) Hashimoto, T.; Shibayama, M.; Kawai, H. *Macromolecules* **1980**, *13*, 1237.
(21) Hashimoto, T.; Nagatoshi, K.; Todo, A.; Hasegawa, H.; Kawai, H. *Macromolecules* **1974**, *7*, 364.

(22) Shibayama, M.; Hashimoto, T. *Macromolecules* **1986**, *19*, 740.
(23) Hasegawa, H.; Hashimoto, T. *Macromolecules* **1985**, *18*, 589.
(24) Inoue, T.; Moritani, M.; Hashimoto, T.; Kawai, H. *Macromolecules* **1971**, *4*, 500.
(25) It is said that there is about 0.3% error in the elementary analysis measurement. This implies that the composition obtained from the elementary analysis involves 7.3% error since the difference in the weight fractions of carbon (or hydrogen) atoms between styrene and isoprene monomeric units is 4.1%. Nevertheless, we believe that the error in the composition is within 1% or 2% when PI content is not so high because the elementary analysis results are reproducible within less than 0.1% of error and also because we usually observe an excellent agreement between the composition thus obtained and that obtained from the analyses of SAXS profiles of lamellar type.[22,26]
(26) Hasegawa, H.; Hashimoto, T. *Kobunshi Ronbunshu*, **1984**, *41*, 759.
(27) This statement may be confusing because in the bulk state solvent removal is more tedious for a material below its T_g than a material above its T_g and at room temperature PS is below its T_g and PI is above its T_g. However, the samples for elemental analysis are usually freeze-dried for faster and more effective removal of the solvent. In this case T_g gives the opposite effect; i.e., PS can maintain a porous structure, which makes solvent removal easier, while a porous structure in PI tends to collapse as the sample temperature increases in the drying process, making complete removal of the solvent very difficult.
(28) Inoue, T.; Soen, T.; Hashimoto, T.; Kawai, H. *J. Polym. Sci., Part A-2* **1969**, *7*, 1283.
(29) Kinning, D. J.; Thomas, E. L.; Alward, D. B.; Fetters, L. J.; Handlin, D. L., Jr. *Macromolecules* **1986**, *19*, 1288.
(30) Helfand, E.; Wasserman, Z. R. In *Developments in Block Copolymers*; Goodman, I., Ed.; Applied Science: Essex, U.K., 1984.
(31) Leibler, L. *Macromolecules* **1980**, *13*, 1602.
(32) Hashimoto, T.; Fujimura, M.; Kawai, H. *Macromolecules* **1980**, *13*, 1660.
(33) Mori, K.; Hasegawa, H.; Hashimoto, T., to be published.
(34) In other words, the occurrence of a morphological transition depends on whether the system is in the strong segregation limit or in the weak segregation limit. According to our unpublished results, the order-disorder transition takes place at ca. 200 °C for PS-PI diblock polymer with $M_n = 3.3 \times 10^4$ and the weight fraction of PS being 0.3. In this case annealing at higher temperatures close to 200 °C might change the morphology (from a nonequilibrium to an equilibrium one). The morphological transition below the order-disorder transition temperature may be possible in some cases if the molecular weights of the block polymers are small. But such a transition is not well understood and left for future investigations.
(35) The thickness of the ultrathin section was measured by the electron microscopy of the folded specimen, the technique proposed by: Adachi, K.; Adachi, M.; Kato, M.; Fukami, A. *Proc. Jpn. Electron Microsc. Soc., 21st* **1965**, 116.
(36) Tilting a specimen under the electron microscope cannot reveal the three-dimensional structure effectively when the thickness of the specimen is smaller than the lattice spacing, since the specimen does not contain the entire unit cell.
(37) This "wagon-wheel" image is different from those reported for the star block polymers simply because the contrast is reversed. However, because of its characteristic appearance we call it also a "wagon-wheel" image.
(38) Hashimoto, T. *Macromolecules* **1982**, *15*, 1548.
(39) Hasegawa, H.; Yamasaki, K.; Hashimoto, T., to be published.
(40) Hasegawa, H.; Hashimoto, T. *Macromolecules* **1985**, *18*, 589.
(41) The order-disorder transition temperature estimated for HY-10 is ca. 550 °C, which is far beyond the degradation temperature of this polymer. Therefore a morphological transition by annealing at a practical temperature cannot be expected for this polymer because the system is in the strong segregation limit and the kinetic barriers are too large.
(42) Burrel, H. *Polymer Handbook*, 2nd ed.; Brandrup, J., Immergut, E. H., Eds.; Wiley: New York, 1975.
(43) Lamellar, cylindrical, and spherical morphologies were successfully obtained from the block polymers having a tetrapod-network structure by changing the selectivity of the casting solvent. However, there has been no success so far in obtaining the tetrapod-network morphology from block polymers having spherical, cylindrical, or lamellar morphology as their equilibrium morphology either by changing the selectivity of the casting solvent or by solubilizing the homopolymer of one component which increases the volume fraction of the corresponding microphase. This may be a key to understanding the physics of the tetrapod morphology and is a subject for future work.
(44) The SAXS intensity distributions for the films cast from toluene, styrene, and 1,4-dioxane are circularly symmetrical with respect to the incident beam axis.
(45) Thomas, E. L.; Kinning, D. J., private communication.
(46) Hasegawa, H.; Hashimoto, T.; Kinning, D. J.; Thomas, E. L.; Fetters, L. J., to be published.
(47) Hasegawa, H., unpublished results.
(48) Unfortunately Figure 12 is reduced in size from the original figure prepared for the stereovision by a factor of 2.2. One should enlarge the picture by this factor for the real stereovision.

Molecular Structure and Elastic Behavior of Poly(ethylene oxide) Networks Swollen to Equilibrium

Yves Gnanou, Gérard Hild, and Paul Rempp*

Institut Charles Sadron (CRM-EAHP) (CNRS-ULP), 67083 Strasbourg Cedex, France.
Received October 6, 1986

ABSTRACT: Poly(ethylene oxide) (PEO) networks are prepared by an end-linking procedure upon reacting α,ω-dihydroxy PEO chains with a plurifunctional isocyanate in stoichiometric amounts. The networks obtained are characterized by their equilibrium swelling degree in dioxane and in water and by the elastic modulus arising from uniaxial compression measurements. For each network, utilizing the Miller-Macosko theory, we have calculated the effective structural parameters, ν, the number of elastically active chains, and μ, the number of junctions, and the trapping factor Te. This enabled us to compare the predictions originating from the various theories of rubber elasticity with our experimental data. It appears that both the limitation of junction fluctuations *and* the trapped entanglements are to be considered to account for the behavior of the swollen PEO networks in the range of small strains.

Introduction

The elastomeric behavior of networks has been investigated for a long time. Much effort has been devoted to relating their elastic response to their molecular structure. The various molecular theories of rubber elasticity rest on the premise that the stress in a deformed elastomer originates from the strain of the elastic chains. The elastic free energy stored (the calculation of which is a key problem) is the sum of contributions of the individual network chains. To test these theories, quantitative and independent information on the structure of the gels (such as molecular weight of the chains, functionality of the cross-links, etc.) is required.

Networks formed by end-linking processes involving reaction between difunctional polymer chains and a plurifunctional cross-linker are relatively well defined.[1] Once

0024-9297/87/2220-1662$01.50/0